Available online at www.sciencedirect.com

ScienceDirect

Geochimica et Cosmochimica Acta xxx (2019) xxx–xxx

Geochimica et Cosmochimica Acta

www.elsevier.com/locate/gca

Rapid mantle convection drove massive crustal thickening in the late Archean

Ming Tang [a,b,*], Cin-Ty A. Lee [a], Roberta L. Rudnick [b,c], Kent C. Condie [d]

[a] Department of Earth, Environmental and Planetary Sciences, Rice University, Houston, TX 77005, USA
[b] Department of Geology, University of Maryland, College Park, MD 20742, USA
[c] Department of Earth Science, University of California at Santa Barbara, Santa Barbara, CA 93106, USA
[d] New Mexico Institute of Mining and Technology, Socorro, NM 87801 USA

Received 18 January 2019; accepted in revised form 30 March 2019; available online xxxx

Abstract

The lithospheric mantle beneath Archean cratons is conspicuously refractory and thick compared to younger continental lithosphere (Jordan, 1988; Boyd, 1989; Lee and Chin, 2014), but how such thick lithospheres formed is unclear. Using a large global geochemical database of Archean igneous crustal rocks overlying these thick cratonic roots, we show from Gd/Yb– and MnO/FeO_T–SiO_2 trends that crustal differentiation required continuous garnet fractionation. Today, these signatures are only found where crust is anomalously thick (60–70 km), as in the Northern and Central Andes and Southern Tibet. The widespread garnet signature in Archean igneous suites suggests that thickening occurred not only in the lithospheric mantle but also in the crust during continent formation in the late Archean. Building thick crust requires tectonic thickening or magmatic inflation rates that can compete against gravitational collapse through lower crustal flow, which would have been enhanced in the Archean when geotherms were hotter and crustal rocks weaker. We propose that Archean crust and mantle lithosphere formed by thickening over mantle downwelling sites with minimum strain rates on the order of 10^{-13}–10^{-12} s^{-1}, requiring mantle flow rates associated with late Archean crust formation to be 10–100 times faster than today.

Keywords: Garnet; Orogeny; Archean; Crustal Evolution; Mantle convection

1. INTRODUCTION

A number of observations indicate that major continental crustal growth may have happened in the Archean. Both detrital zircon U-Pb ages (e.g., Voice et al., 2011; Parman, 2015) and mantle xenolith Re depletion model ages (e.g., Carlson et al., 2005; Pearson et al., 2007; Griffin et al., 2014) show prominent peaks between 2.5 and 3.0 Ga. Transition metal chemistry of terrigenous sedimentary rocks supports conclusions made from mantle xenolith and detrital zircon observations, suggesting a rapid change in crust composition (Tang et al., 2016) and massive subaerial crust expansion (Bindeman et al., 2018) in the late Archean [Note that recent work on the Ti isotopes of shales suggested an Archean crust dominated by felsic rocks (Greber et al., 2017), though this interpretation is now complicated by the recognition that Ti isotopes do not follow a single igneous differentiation trend (Deng et al., 2019)].

The mechanism(s) that drove this rapid continental crust growth remains largely unknown. Although mantle melting provides the "building blocks" for the crust, the formation and differentiation of the continental crust, which has an intermediate, calc-alkaline average composition (Kelemen, 1995), appear to be closely related with orogenic processes (Lee et al., 2007; Karlstrom et al., 2010; Ducea et al., 2015;

* Corresponding author at: Department of Earth, Environmental and Planetary Sciences, Rice University, Houston, TX 77005, USA.
E-mail address: tangmyes@gmail.com (M. Tang).

https://doi.org/10.1016/j.gca.2019.03.039
0016-7037/

Tang et al., 2018; Tang et al., 2019). Coupling continental crust formation and orogenic processes in early Earth is challenging because orogens are readily destroyed by gravitational collapse, erosion and weathering. To probe ancient orogenic processes, we studied garnet-sensitive geochemical indices in Archean igneous differentiation suites.

Garnet appears on the liquid line of descent only at relatively high pressures. For example, in granitic melts, garnet crystallizes at 0.8–1.0 GPa (Moyen and Stevens, 2013); in andesitic melts, garnet crystallizes at ≥1.2 GPa (Alonso-Perez et al., 2009); in basaltic melts, the pressure at which garnet crystallizes appears to be ≥2 GPa (Green, 1982; Elthon and Scarfe, 1984; Presnall, 1999). Magmatic garnet-bearing cumulates have been observed in the exposed lower sections of thickened arc crust in the Sierra Nevada (USA) (Lee et al., 2006) and Kohistan (Ringuette et al., 1999; Jagoutz and Schmidt, 2013). During melting or crystallization, the presence of garnet in the residual/crystallizing assemblage will impart distinctive geochemical signatures to the magmas. For example, heavy rare earth element and Mn concentrations are sensitive to garnet because these elements strongly partition into it (Fujimaki et al., 1984; Rudnick and Taylor, 1986; Pertermann et al., 2004). Combining these diagnostic garnet geochemical signatures with P-T constraints on garnet stability offers the possibility to track crustal thickness through the compositional changes accompanying igneous differentiation. Here we apply this method to Archean igneous rocks and show that garnet signatures dominate the entire Archean igneous differentiation spectrum (from basalt to granite) and that this signature largely disappears after the Archean, except in regions of anomalously thick crust.

2. SAMPLES AND METHODS

The Archean database ($n = 11{,}627$) used here combines the database used by Tang et al. (2016) and our updated compilation of Archean granitoids. This database, which is available in the Supplementary file, incorporates samples that experienced various degrees of metamorphism including Archean gray gneisses. We did not remove these gneisses, as their MnO/FeO_T and REE ratio signatures should largely reflect their igneous origins. We excluded komatiite, lamprophyre, kimberlite, harzburgite, peridotite, phonolite and wehrlite from the database when plotting and discussing Archean igneous differentiation because they are not significant components of continental crust. The modern arc database ($n = 36{,}947$) is taken from Farner and Lee (2017), which only incorporates Pleistocene to Holocene age volcanic rocks so that the rock compositions reflect the crustal thickness when the lavas erupted. When calculating the SiO_2 binned mean values, we filtered out samples falling within the highest 10% of the ratio of interest (e.g., $[Gd/Yb]_N$, MnO/FeO_T), as well as samples falling within the lowest 10%. Adding these extreme samples back will increase the uncertainties, but has no effect on the average differentiation trends.

3. RESULTS

3.1. Prevalent garnet fractionation signatures in Archean igneous suites

As magmas differentiate from mafic to felsic compositions, fractionation between middle and heavy REEs (MREE/HREE) is controlled by crystallization of amphibole, garnet, and accessory phases such as apatite. Amphibole and apatite fractionation result in decreasing MREEs/HREEs ratios in the magma because both phases preferentially take up MREEs; garnet fractionation, however, depletes HREEs and increases the MREEs/HREEs ratio in the magma (Fujimaki et al., 1984; Rudnick and Taylor, 1986; Davidson et al., 2013). Garnet fractionation is reflected in distinct $Gd/Yb–SiO_2$ relationships in modern arcs with high elevation volcanos that are built on thick crust (Fig. 1a). Likewise, $MnO/FeO_T–SiO_2$ relationships (the subscript T denotes total iron content in the form of FeO) also record crustal thickness via garnet fractionation. At low pressure, oxide fractionation depletes Fe in magmas (Zimmer et al., 2010; Tang et al., 2018) but has little effect

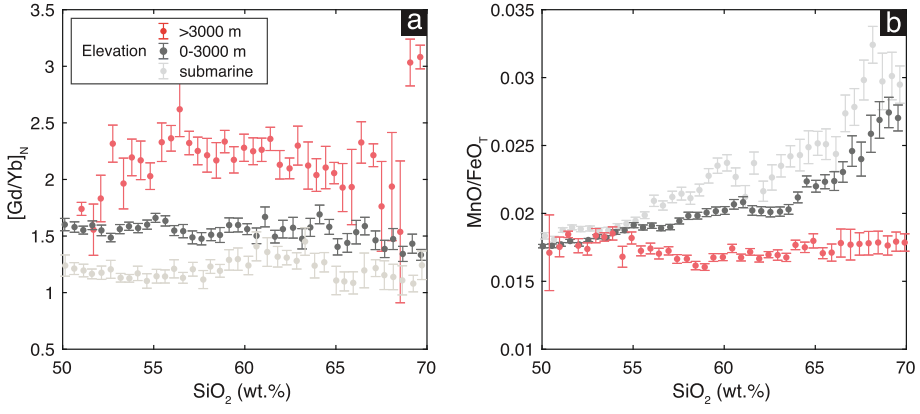

Fig. 1. $[Gd/Yb]_N$– and $MnO/FeO_T–SiO_2$ trends in modern arc volcanic rocks. The samples are grouped by their elevation (submarine, 0–3000 m and >3000 m), which reflects the local crustal thickness (Lee et al., 2015), and are plotted as mean and two standard error uncertainties as a function of SiO_2 in 0.5 wt.% increments. $[Gd/Yb]_N$ denotes chondrite (Sun and McDonough, 1989) normalized Gd/Yb ratio. Scatter plots are provided in the Supplementary file.

Please cite this article in press as: Tang M., et al. Rapid mantle convection drove massive crustal thickening in the late Archean. *Geochim. Cosmochim. Acta* (2019), https://doi.org/10.1016/j.gca.2019.03.039

on Mn (see Supplementary file for compiled Fe and Mn partition coefficients), resulting in an increasing MnO/FeO_T ratio with differentiation in most arcs (Fig. 1b). However, when garnet fractionation is involved, as would be the case for high-pressure differentiation, the strong partitioning of Mn and Fe into garnet (see Supplementary file) causes rapid depletion of both elements in the melt, leading to nearly constant MnO/FeO_T ratio with differentiation (Fig. 1b).

Today, garnet-dominated differentiation is only observed in high elevation areas (>3000 m) (Fig. 1), such as the Central-Northern Andes where the crust is 60–70 km thick. By contrast, these garnet signatures appear to be the norm in Archean igneous differentiation suites and are evident in all major Archean cratons (Fig. 2). Although the tectonic settings are poorly constrained for many Archean igneous suites and unravelling intracrustal differentiation processes is complicated, the garnet signatures inferred from the Gd/Yb and MnO/FeO_T–SiO_2 trends largely reflect the pressure of igneous differentiation at that time.

We note that there is a difference between the Gd/Yb-SiO_2 trends of the Archean igneous rocks and modern arcs with thick crust as the magmas become more silicic. The samples from modern arcs with thick crust show increasing Gd/Yb with differentiation until SiO_2 reaches ~56 wt.%, after which Gd/Yb remains constant with further differentiation; in the Archean igneous suites, however, the Gd/Yb keeps increasing throughout the SiO_2 range (Fig. 2a). We suggest this could be due to a difference in sampling depth between the two groups. Because modern arc samples used here are young (<2.58 Ma) volcanic rocks, they reflect both high-pressure lower crust and low-pressure upper crust differentiation signatures imparted as magmas ascend and differentiate in thick arc crust. Amphibole fractionation at shallower depth decreases Gd/Yb, which suppresses the garnet signature during late stage differentiation. By contrast, in the Archean igneous suites, felsic samples are dominated by tonalite-trondhjemite-granodiorite (TTG) intrusive rocks, most of which equilibrated with garnet-bearing residues at great depths (Moyen and Martin, 2012). Considering the rapid surface erosion during orogenic processes (Roering et al., 2007), it is possible that the preserved Archean igneous suites are biased, because shallow volcanic rocks from the ancient upper crust that experienced low pressure differentiation are missing. This argument is speculative and should be further tested, but the decreasing average Gd/Yb from volcanic to plutonic rocks in the Kohistan arc appears to support this hypothesis (see Supplementary file).

3.2. The origin of the garnet fractionation signatures in Archean igneous differentiation

Of interest here is the origin the garnet fractionation signature. One possibility is that it is generated by partial melting of subducted oceanic crust, leaving behind a garnet-bearing eclogitic slab residue (Martin, 1986). Many Archean TTGs have been suggested to be slab melts (Martin and Moyen, 2002). However, it seems unlikely that slab melting could impart a garnet signature across the entire compositional spectrum of Archean igneous rocks, as generating a basaltic andesite melt from a basaltic source would require >50% melting (Pertermann and Hirschmann, 2003), diluting any effect of garnet in the residue. Furthermore, modern magmas that may derive from slab melting

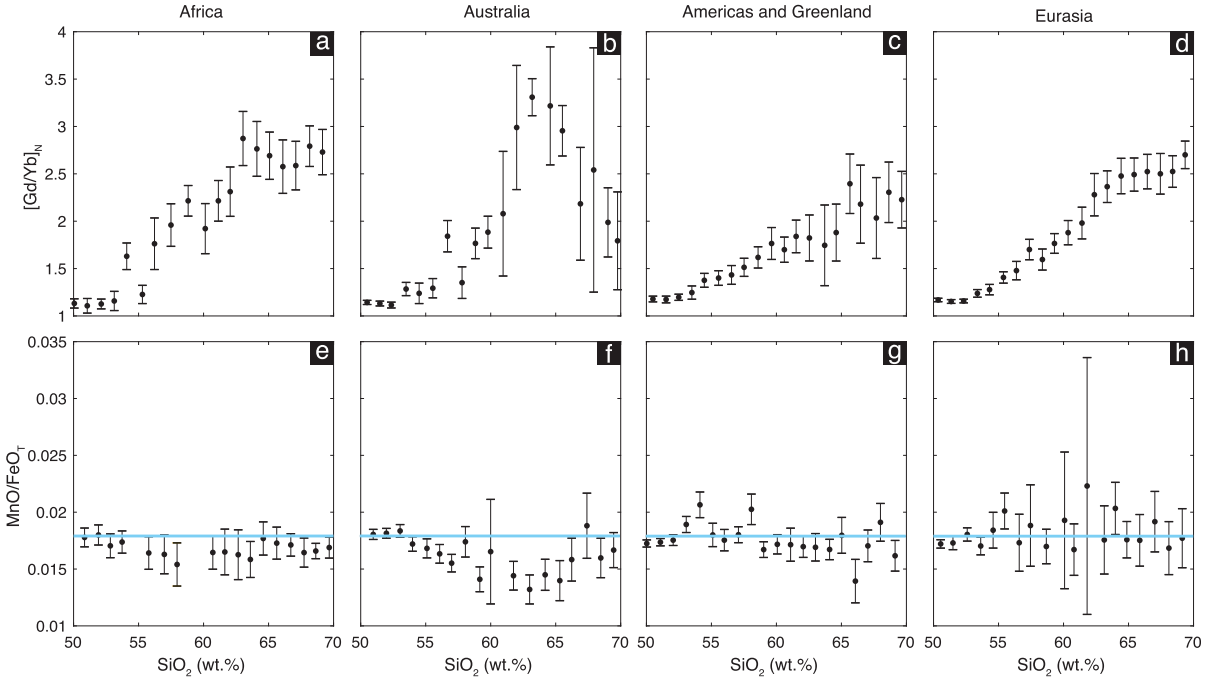

Fig. 2. $[Gd/Yb]_N$– and MnO/FeO_T–SiO_2 trends in Archean igneous rock suites. Shown in the plots are mean and two standard error uncertainties for samples as functions of SiO_2 in 1 wt.% increments. Scatter plots are provided in Supplementary file.

(e.g., many adakites) usually have Mg#s (atomic ratio $Mg/(Mg + Fe_T)$) high enough to be near equilibrium with peridotitic mantle, despite their felsic compositions (Martin et al., 2005). The high Mg# in otherwise intermediate magmas is a signature of interaction of silicic slab melts with mantle peridotite in the mantle wedge. This high Mg# signature is not observed in Archean intermediate rocks (Fig. 3). Instead, Archean igneous differentiation mimics that seen in the Andean arc magmas, where igneous differentiation is largely driven by crystal fractionation in the crust (Lee and Bachmann, 2014). The lack of high Mg#s in the Archean andesitic rocks suggests that most of the Archean intermediate magmas never interacted with mantle peridotites, and were therefore not formed by slab melting, but rather by intracrustal differentiation.

It is also possible that these apparent garnet-differentiation trends are artifacts of magma mixing between basalts and slab-derived TTG melts, but a mixing origin is not supported by P_2O_5–SiO_2 systematics (Lee and Bachmann, 2014). Mixing between felsic and mafic magmas should generate linear arrays in P_2O_5–SiO_2 space, but the Archean igneous suites define an arcuate array, which is more consistent with crystal fractionation, wherein magmas are initially under-saturated in apatite and therefore exhibit an initial increase in P_2O_5 with increasing SiO_2 until the magma reaches apatite saturation, after which P_2O_5 decreases with further differentiation (Lee and Bachmann, 2014) (Fig. 4).

We conclude that the garnet signatures seen in Archean igneous rocks, at least those representing basaltic to andesitic differentiation ($SiO_2 = 50$–60 wt.%), were most likely produced by high-pressure igneous differentiation in a thick crust. The similarity of $[Gd/Yb]_N$– and MnO/FeO_T–SiO_2 trends between the Archean and central-northern Andes igneous suites suggests that orogenic processes were prevalent in the Archean. It is worth noting that our Archean igneous database is dominated by samples with ages between 2.7 and 3.1 Ga (Fig. 5). Therefore, the thick crust inferred from garnet signatures related to igneous differentiation may be restricted to the late Archean. To determine whether massive crustal thickening also occurred in the early Archean will require many more analyses of >3.0 Ga samples (see Fig. S4 in the Supplementary file for plots that delineate late Archean (2.5–3.0 Ga) vs. older samples).

4. DISCUSSION

4.1. Geothermal gradients in thick Archean crust

Owing to higher mantle heat flux and higher amounts of radioactivity earlier in Earth's history, it seems reasonable to expect the Archean crust to be hotter than today's crust for any given composition. Here we calculate the geothermal gradients for a 70 km thick crust and underlying lithospheric mantle at 3.0 Ga assuming steady state

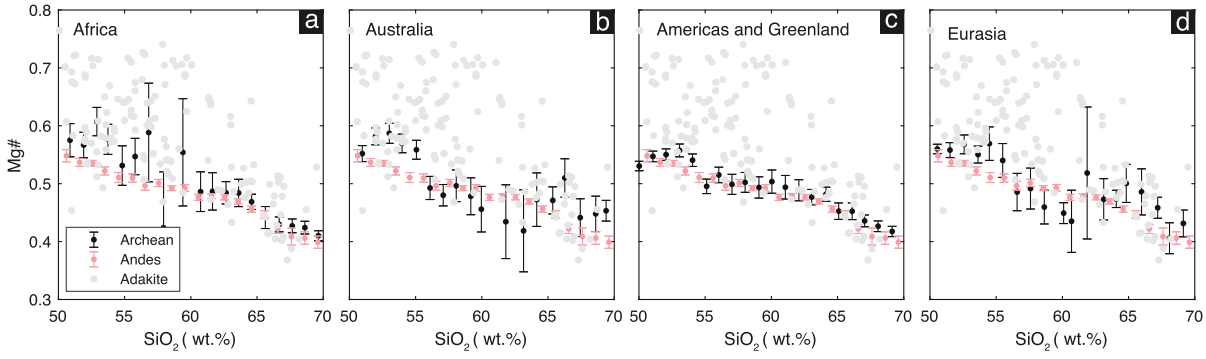

Fig. 3. Average Mg#–SiO_2 trends in Archean and Andean arc igneous differentiation compared with Cenozoic adakites. Archean and Andean arc data are plotted as SiO_2 binned average Mg#. Errors bars are two standard error of mean; Cenozoic adakites are plotted as individual samples. The compiled adakite data are provided in the Supplementary file.

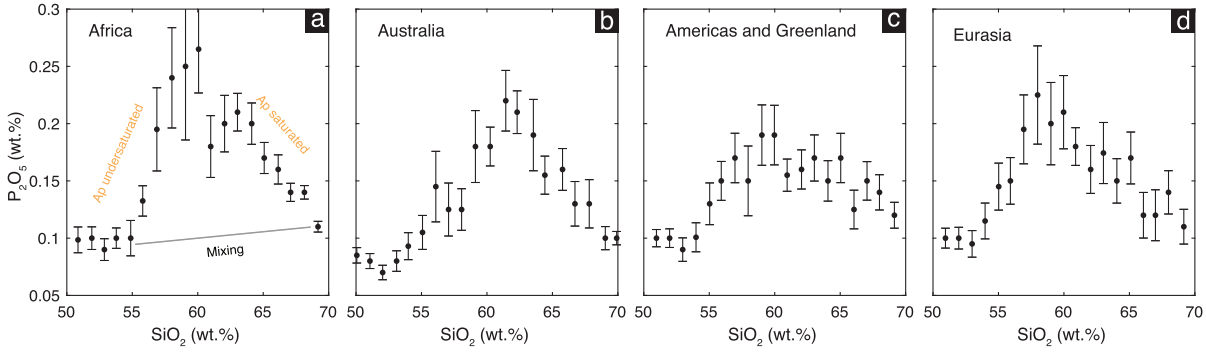

Fig. 4. Average P_2O_5–SiO_2 trends in Archean igneous differentiation. Data are plotted as SiO_2 binned average P_2O_5 contents. "Ap" is apatite. Errors bars are two standard error of mean.

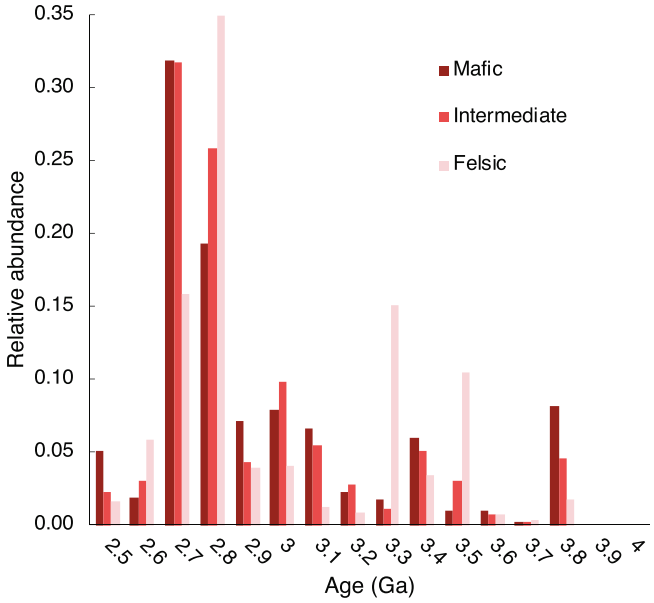

Fig. 5. Age distribution of Archean mafic, intermediate and felsic igneous rocks from the geochemical database. Not all samples in our dataset have radiometric ages. We assume that the samples with radiometric ages (56% of the total) are representative of the age distribution of the entire dataset.

conductive heat transfer. We searched for the coldest geotherms that intersect the Archean mantle adiabat with a surface potential temperature of 1550 °C (1823 K) (Herzberg et al., 2010).

$$\frac{D^2T}{dz^2} = -\frac{A}{k} \tag{1}$$

where T is temperature (K), z is depth (m), A is volumetric heat production in (W m^{-3}) and k is thermal conductivity in (W m^{-1} K^{-1}). The volumetric heat production in the crust is:

$$A_j = \sum_j F_j \rho \sum_i H^i C_j^i e^{-\lambda^i t} \tag{2}$$

where $i = {}^{40}$K, ^{232}Th, ^{235}U and ^{238}U, j indicates mafic and felsic crust, F is volumetric proportion, ρ is the density (2800 kg m^{-3}), λ^i is the decay constant (yr^{-1}), t is time before present (yr), H^i is heat production (μW m^{-3}), C^i is the present-day concentration. To calculate heat production, we only considered samples having complete data for K_2O, Th and U, and filtered out the highest 10% and lowest 10% (as described above). Archean mafic rocks (SiO_2 = 40–52 wt.%) have average K_2O, Th and U concentrations of 0.29 ± 0.01 wt.%, 0.52 ± 0.02 ppm and 0.15 ± 0.01 ppm (2 se), respectively, which are not significantly different from the median concentrations (0.27 wt.%, 0.50 ppm and 0.15 ppm for K_2O, Th and U, respectively). The average concentrations give average K/U and Th/U ratios of 16,042 and 3.5, respectively. We used these average K_2O, U and Th concentrations as representative of Archean mafic crust. For felsic crust, we took the average K_2O, Th and U concentrations in TTG reported by Moyen and Martin (2012), which are 1.7 wt.%, 5.72 ppm and 1.42 ppm, respectively, yielding K/U = 9934 and Th/U = 4.0, respectively. Volumetric heat production in the Archean lithospheric mantle was set at 0.04 μW m^{-3}, which is roughly twice that observed today in lithospheric mantle beneath Archean cratons (Rudnick et al., 1998). The thickness of the lithospheric mantle is determined such that the coldest conductive geothermal gradient (minimum Moho heat flux q_m) intersects the adiabatic geothermal gradient at <250 km. Thermal conductivity k is temperature and pressure dependent. Following Chapman (1986), we let

$$k_j|_{T,z} = \frac{k_{j,0}(1 + c_j z)}{1 + b_j(T - 273K)} \tag{3}$$

$$k|_{T,z} = \sum_j F_j k_j|_{T,z} \tag{4}$$

where k_0 is the thermal conductivity measured at 0 °C and one atmosphere pressure. For mafic crust, $k_0 = 2.6$ W m^{-1} K^{-1}, $b = 1.0 \times 10^{-4}$ K^{-1}, and $c = 1.5 \times 10^{-3}$ km^{-1}; for felsic crust, $k_0 = 3.0$ W m^{-1} K^{-1}, $b = 1.5 \times 10^{-3}$ K^{-1}, and $c = 1.5 \times 10^{-3}$. Thermal conductivity in the mantle was assigned as a constant of 3.4 W m^{-1} K^{-1}. We considered the Moho heat flux q_{moho} in the range of 0–50 mW m^{-2}, and

$$dq = Adz \tag{5}$$

The calculated geothermal gradients are shown in Fig. 6a. The Archean crust becomes significantly hotter with increasing amounts of TTG in the crust. Even with minimum mantle heat flux, the temperature can readily reach 1000 °C or higher at the Moho of a 70 km thick Archean crust. At such high temperature, the lower part of the thick Archean crust is likely melt-bearing with weak rheology.

In summary, the geochemical data show conclusively that Archean igneous rocks formed in a thick crust where garnet was stable, yet such a thick crust at that time would

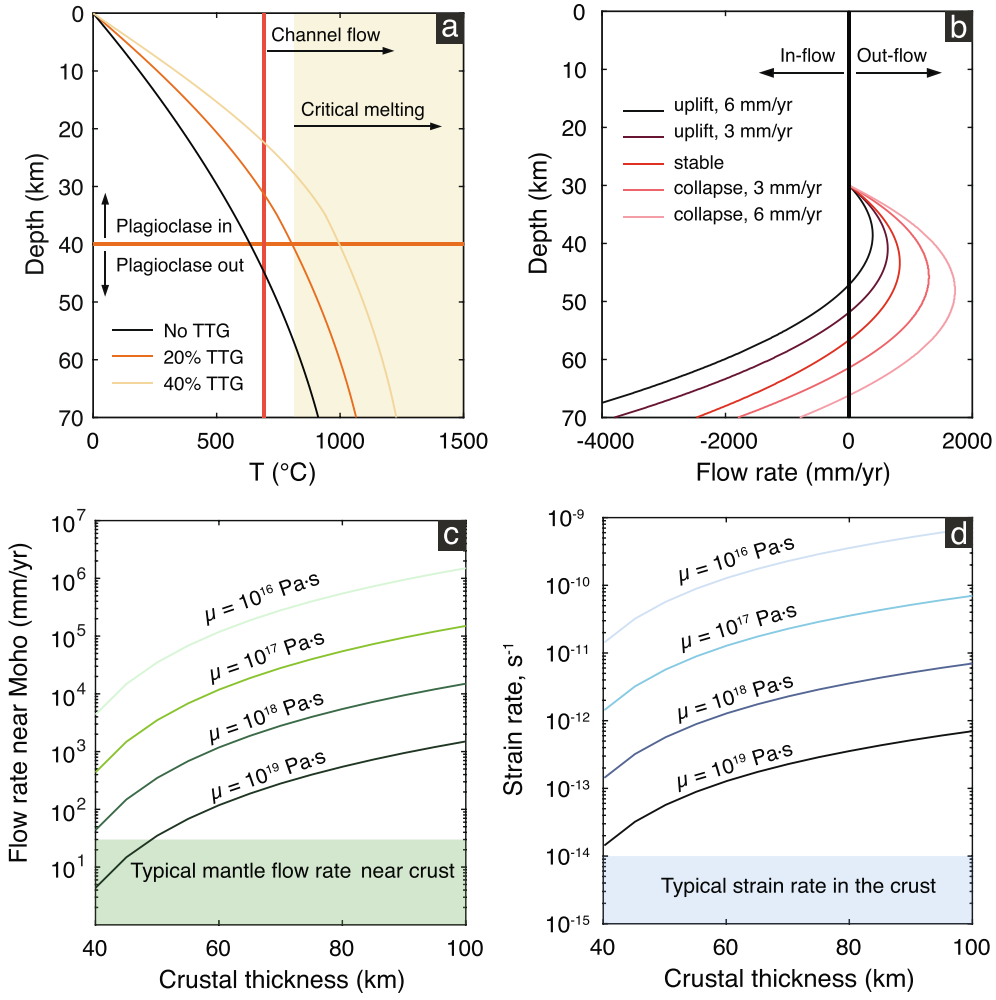

Fig. 6. Calculated thermal structure and rheology of the Archean thickened crust. (a) Minimum steady state geothermal gradients with 0–40% TTG in the upper half of the thickened crust. With over 20% TTG by volume in the upper 35 km, the crust reaches typical crustal dehydration melting temperature in the plagioclase stability field. (b) Depth profiles of crustal flow velocity at uplifting, stable, and collapsing stages. (c and d), Crust/mantle flow velocity near Moho and strain rate of crustal deformation as functions of total crustal thickness and effective viscosity in the flow channel.

be inherently weak due to its radioactivity. These observations highlight the need for tectonic compression, related to plate convergence and orogeny, to maintain a thick and hot crust at the end of the Archean. In the next section, we use these observations to place constraints on the magnitude of the strain rates that are required to produce such a thickened crust, and speculate about what internal processes may have given rise to such high stain rates.

4.2. Constraints on mantle convection rates in the late Archean

Given that hot crust is weak, gravitational collapse through lower crustal flow would be more efficient (Kruse et al., 1991; Clark and Royden, 2000; Jamieson et al., 2011; Wang et al., 2012), potentially limiting the thickness and elevation of Archean crust. Such thermal weakening could be reduced if the amounts of radiogenic isotopes in the crust were low, as would be the case for a dominantly mafic crust (Fig. 6a). But this alone may not be sufficient to maintain a thick crust if heat flow was high in the past, or if crustal thickening was also associated with magmatism, a source of advective heat. What seems necessary is a process by which this weak but thickened crust was supported by tectonic compression, as occurs in modern orogenic belts. Clues to this process may come from the inferred pressure increases observed in Archean cratonic peridotites. The subsolidus pressures of Archean cratonic peridotites are 1–2 GPa (30–60 km) higher than their igneous protolith pressures (Lee and Chin, 2014). It seems that Archean mantle peridotites were first melted and depleted at shallow depths, and then transported to greater depths beneath Archean cratons. Such a process could happen at mantle downwelling sites, where convergent mantle flow generates lateral compression (Fig. 7).

To estimate the magnitude of such compression, we consider a simple model by which crustal thickening is driven by basal shear via mantle downwelling (Fig. 7). We use

Please cite this article in press as: Tang M., et al. Rapid mantle convection drove massive crustal thickening in the late Archean. *Geochim. Cosmochim. Acta* (2019), https://doi.org/10.1016/j.gca.2019.03.039

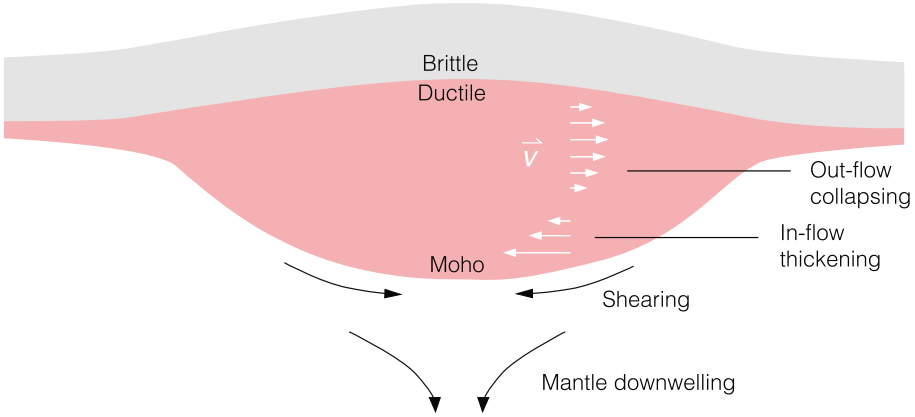

Fig. 7. Cartoon (not to scale) showing lithospheric thickening at mantle downwelling sites. Mantle downwelling occurs as a result of negative buoyancy due to cooling. Mantle downwelling propagates lateral shear to the crust and drives crustal thickening. As the crust thickens, its elevation increases, which induces gravitational collapse through mid to lower crustal flow. Steady-state crustal thickness is reached when the power of crustal thickening equals that of gravitational collapse. Mantle overturn is one possible scenario that results in extremely fast mantle convection and causes large-scale orogenic processes and topographic change at the surface. The remnants of the downwelling mantle might have formed the thick lithospheric mantle found beneath Archean cratons that we observe today.

Couette and Poiseuille flow models to approximate crustal thickening and collapsing processes, respectively. Because the crust generally reaches the critical temperature for channel flow at ~30 km (Fig. 6a), we assume that the top of the lower crustal channel is at 30 km depth. Assuming lower crustal flow is coupled to mantle flow, the mantle-driven lower crustal flow rates can be approximated using Couette flow:

$$v_c = v_m\left(1 - \frac{z}{h}\right) \tag{6}$$

where z is vertical distance from the Moho; v_m is the lower crustal flow velocity at Moho, h is the thickness of the low viscosity channel and v_c is the flow velocity in the channel at z. Crustal collapse through a lower crustal "channel" can be approximated by Poiseuille flow (Turcotte and Schubert, 1982):

$$v_p = -\frac{1}{2\mu}\frac{dp}{dx}(z^2 - hz) \tag{7}$$

where v_p is the flow velocity; μ is viscosity in the channel, which was assumed to be constant; p is differential pressure and x is lateral distance. The pressure gradient is controlled by topography (T_h), such that:

$$\frac{dp}{dx} = \frac{2\rho_c g T_h}{L} \tag{8}$$

where L is the width of the convergent region. T_h is given by Airy isostatic equilibrium:

$$T_h = \Delta H\left(1 - \frac{\rho_c}{\rho_m}\right) \tag{9}$$

where ρ_m and ρ_c are densities of mantle (3300 kg/m^3) and crust (2800 kg/m^3) and ΔH is the difference in thickness between the thickened (=70 km) and reference crust (30 km, (Herzberg and Rudnick, 2012). We set the width of the orogen (L) to an upper bound of 1000 km. The narrower the orogen, the greater the pressure gradient will be for a given elevation or crustal thickness. We can define the minimum basal shear stress needed to support an excess crustal thickness of ΔH by equating the thickening and collapsing fluxes, $U_{collapsing} = U_{thickening}$:

$$\int_0^h v_c dz + \int_0^h v_p dz = 0 \tag{10}$$

Solving equations (7)–(11), we obtain the minimum crustal strain rate $\dot{\varepsilon}$ or mantle velocity v_m at the base of the crust:

$$\dot{\varepsilon} \sim \frac{v_m}{h} \sim \frac{\rho_c g h \Delta H}{3\mu L}\left(1 - \frac{\rho_c}{\rho_m}\right) \tag{11}$$

The above equation shows that high strain rates are needed to support thickened crust. For a 70 km thick crust in the Archean and reasonable geotherms (assuming a minimum basal heat flux), the crust is hot. With over 20% of the upper crust as TTG, partial melting of the crust can occur at 25–40 km depth (Fig. 6a), and the weak lower crustal channel might be as thick as ~40 km. Typical effective viscosity in a melt-bearing lower crustal channel is on the order of 10^{18}–10^{19} Pa s^{-1}, and may be further reduced with increasing temperature and/or melt fraction (Kruse et al., 1991; Clark and Royden, 2000; Husson and Sempere, 2003; Jamieson et al., 2011). The lower part of the thickened Archean crust can reach >1000 °C and is likely melt-bearing even if the composition is mafic. Under these conditions, crustal and mantle strain rates are on the order of 10^{-13}–10^{-12} s^{-1}, corresponding to "plate" velocities of 10^2–10^3 mm/yr (Fig. 6d). These crustal strain rates and velocities are 10–100 times higher than today's. We did not consider erosion and lower crustal foundering in the model, both of which would result in crustal thinning. Lower crustal foundering also drives the bulk crust composition from mafic to felsic (Kay and Mahlburg-Kay, 1991; Rudnick and Fountain, 1995; Rudnick, 1995; Lee, 2014; Tang et al., 2015). If erosion and lower crustal foundering

Please cite this article in press as: Tang M., et al. Rapid mantle convection drove massive crustal thickening in the late Archean. *Geochim. Cosmochim. Acta* (2019), https://doi.org/10.1016/j.gca.2019.03.039

were operative, it would lead to even greater crustal thickening rates, thus higher crust and mantle strain rates, as implied in our model.

The occurrence of thick continental crust in the Archean requires more rapid mantle convergence rates, which likely occur preferentially over mantle downwellings (Cooper and Miller, 2014; Wang et al., 2016). Because most of the Archean igneous samples compiled here have ages younger than 3.0 Ga (Fig. 5), we cannot determine whether rapid convergence characterized the entirety of the Archean, or whether it reflects an unusual pulse in the late Archean. More vigorous mantle convection throughout the Archean is consistent with higher mantle temperatures in the past (Christensen, 1985; Herzberg et al., 2010), although it has been also proposed that plates would be more sluggish on a hotter Earth (Korenaga, 2013). Rapid convergence could also be the result of major mantle overturn events (Christensen and Yuen, 1985; Tackley et al., 1993; Stein and Hofmann, 1994; Breuer and Spohn, 1995; O'Neill et al., 2007; Crameri and Tackley, 2016). Such major mantle overturn events may have been the driver of accelerated continental crust formation in the late Archean due to extensive partial melting and formation of mafic crust above upwelling zones, followed by massive crustal thickening and differentiation of such crust over downwellings (e.g., Stein and Hofmann, 1994). We speculate that a major mantle overturn might serve as a stimulus to initiate plate tectonics (Crameri and Tackley, 2016), with spreading centers forming above upwelling sites and subduction initiated near downwelling sites. Whether the massive orogenic processes recognized here represent a prelude or response to the initiation of plate tectonics cannot be determined from our data. If plate tectonics was operating in the late Archean, an interesting question is the role of slab pull. High melting degrees may generate much thicker oceanic crust in the Archean (Herzberg and Rudnick, 2012). Subduction of this thick oceanic crust at convergent margins may generate stronger slab pull than in modern subduction zones, and how this enhanced slab pull would contribute to mantle convection and orogenic processes in the upper plate awaits future studies.

Interpreting the geologic record of the Archean orogenic processes is generally non-unique and ancient orogens may not be well preserved due to rapid erosion and gravitational collapse. We suggest that after the passage of a mantle overturn event, mantle convection rates decrease, diminishing lateral compressive forces in the crust, which results in the gradual gravitational collapse of the thickened crust. However, the underlying mantle lithosphere that was significantly melted at shallow depths, and then thickened during rapid mantle downwelling, may survive and be preserved as the thick mantle keels observed today beneath ancient cratons–the core of continents (Boyd, 1989; Jordan, 1988).

4.3. Implications for atmospheric oxygenation

Vigorous orogenic processes can have profound influences on surface dynamics in the Archean, including enhanced chemical weathering, organic carbon burial, hydrologic cycle, etc. Magmatic orogens serve as both a source and sink of CO_2 through magmatic degassing and enhanced erosion/weathering, causing greenhouse/icehouse effects (Lee et al., 2013; Lee and Lackey, 2015; Lee et al., 2015; McKenzie et al., 2016). Orogeny may increase organic carbon burial efficiency, and induce pulsed atmospheric oxygenation (Campbell and Allen, 2008; Planavsky, 2018), which may explain the "whiffs of oxygen" in the late Archean (Anbar et al., 2007). Perhaps more importantly, the changes in crust composition (Tang et al., 2016), and the expansion of subaerial crust (Bindeman et al., 2018) and continental shelf areas following orogeny may fundamentally shift the long-term balance between oxygen production through photosynthesis and oxygen consumption through oxidative reactions (Husson and Peters, 2017).

5. CONCLUSIONS

Archean igneous rocks show prominent garnet fractionation signatures from basalt to granite, namely, rising Gd/Yb and constant MnO/FeO_T with increasing SiO_2 content. Such garnet signatures were likely formed during intracrustal differentiation (crystal fractionation and/or crustal remelting) rather than subducted slab melting because of the lack of high Mg# in the majority of the differentiated samples. These garnet signatures are seen in igneous rocks from all major Archean cratons, suggesting widespread orogenic processes in the Archean.

To support a thick continental crust and drive such vigorous orogenic processes in the Archean, the strain rate of the convecting Archean upper mantle was at least an order of magnitude higher than today and may have been the manifestation of mantle overturn towards the end of the Archean.

ACKNOWLEDGEMENTS

This project was supported by Frontiers of Earth Systems and Dynamics NSF OCE-1338842, University of Maryland Research Funds to R.L.R., a Wylie Dissertation Fellowship to M.T., and NSF grant EAR 0948549. We appreciate discussions with William McDonough, Balz Kamber, and Taras Gerya. We thank Claude Herzberg, Nicholas Arndt, and five anonymous reviewers for their insightful reviews.

APPENDIX A. SUPPLEMENTARY MATERIAL

Supplementary data to this article can be found online at https://doi.org/10.1016/j.gca.2019.03.039.

REFERENCES

Alonso-Perez R., Müntener O. and Ulmer P. (2009) Igneous garnet and amphibole fractionation in the roots of island arcs: experimental constraints on andesitic liquids. *Contrib. Miner. Petrol.* **157**, 541–558.

Anbar A. D., Duan Y., Lyons T. W., Arnold G. L., Kendall B., Creaser R. A., Kaufman A. J., Gordon G. W., Scott C., Garvin J. and Buick R. (2007) A whiff of oxygen before the great oxidation event? *Science* **317**, 1903–1906.

Bindeman I. N., Zakharov D. O., Palandri J., Greber N. D., Dauphas N., Retallack G. J., Hofmann A., Lackey J. S. and Bekker A. (2018) Rapid emergence of subaerial landmasses and onset of a modern hydrologic cycle 2.5 billion years ago. *Nature* **557**, 545–548.

Boyd F. R. (1989) Compositional distinction between oceanic and cratonic lithosphere. *Earth Planet. Sci. Lett.* **96**, 15–26.

Breuer D. and Spohn T. (1995) Possible flush instability in mantle convection at the Archaean-Proterozoic transition. *Nature* **378**, 608–610.

Campbell I. H. and Allen C. M. (2008) Formation of supercontinents linked to increases in atmospheric oxygen. *Nat. Geosci.* **1**, 554.

Carlson R. W., Pearson D. G. and James D. E. (2005) Physical, chemical, and chronological characteristics of continental mantle. *Rev. Geophys.* **43**, RG1001.

Chapman D. S. (1986) Thermal gradients in the continental crust. *Geol. Soc. London, Special Publ.* **24**, 63–70.

Christensen U. R. (1985) Thermal evolution models for the Earth. *J. Geophys. Res. Solid Earth* **90**, 2995–3007.

Christensen U. R. and Yuen D. A. (1985) Layered convection induced by phase transitions. *J. Geophys. Res. Solid Earth* **90**, 10291–10300.

Clark M. K. and Royden L. H. (2000) Topographic ooze: Building the eastern margin of Tibet by lower crustal flow. *Geology* **28**, 703–706.

Cooper C. and Miller M. (2014) Craton formation: Internal structure inherited from closing of the early oceans. *Lithosphere* **6**, 35–42.

Crameri F. and Tackley P. J. (2016) Subduction initiation from a stagnant lid and global overturn: new insights from numerical models with a free surface. *Prog. Earth Planet. Sci.* **3**, 30.

Davidson J., Turner S. and Plank T. (2013) Dy/Dy*: variations arising from mantle sources and petrogenetic processes. *J. Petrol.* **54**, 525–537.

Deng Z., Chaussidon M., Savage P., Robert F., Pik R. and Moynier F. (2019) Titanium isotopes as a tracer for the plume or island arc affinity of felsic rocks. *Proc. Natl. Acad. Sci.*, 201809164.

Ducea M. N., Saleeby J. B. and Bergantz G. (2015) The architecture, chemistry, and evolution of continental magmatic arcs. *Annu. Rev. Earth Planet. Sci.* **43**, 299–331.

Elthon D. and Scarfe M. C. (1984) High-pressure phase equilibria of a high-magnesia basalt and the genesis of primary oceanic basalts. *Am. Mineral.* **69**, 1–15.

Farner M. J. and Lee C.-T. A. (2017) Effects of crustal thickness on magmatic differentiation in subduction zone volcanism: a global study. *Earth Planet. Sci. Lett.* **470**, 96–107.

Fujimaki H., Tatsumoto M. and Aoki K.-I. (1984) Partition coefficients of Hf, Zr, and REE between phenocrysts and groundmasses, Lunar. In *and Planetary Science Conference Proceedings*, pp. B662–B672.

Greber N. D., Dauphas N., Bekker A., Ptáček M. P., Bindeman I. N. and Hofmann A. (2017) Titanium isotopic evidence for felsic crust and plate tectonics 3.5 billion years ago. *Science* **357**, 1271–1274.

Green T. H. (1982) Anatexis of mafic crust and high pressure crystallization of andesite. In *Andesites: Orogenic Andesites and Eelated Rocks* (ed. R. S. Thorpe). John Wiley & Sons, New York, pp. 465–487.

Griffin W. L., Belousova E. A., O'Neill C., O'Reilly S. Y., Malkovets V., Pearson N. J., Spetsius S. and Wilde S. A. (2014) The world turns over: hadean-Archean crust–mantle evolution. *Lithos* **189**, 2–15.

Herzberg C., Condie K. and Korenaga J. (2010) Thermal history of the Earth and its petrological expression. *Earth Planet. Sci. Lett.* **292**, 79–88.

Herzberg C. and Rudnick R. (2012) Formation of cratonic lithosphere: an integrated thermal and petrological model. *Lithos* **149**, 4–15.

Husson J. M. and Peters S. E. (2017) Atmospheric oxygenation driven by unsteady growth of the continental sedimentary reservoir. *Earth Planet. Sci. Lett.* **460**, 68–75.

Husson L. and Sempere T. (2003) Thickening the Altiplano crust by gravity-driven crustal channel flow. *Geophys. Res. Lett.*, 30.

Jagoutz O. and Schmidt M. W. (2013) The composition of the foundered complement to the continental crust and a re-evaluation of fluxes in arcs. *Earth Planet. Sci. Lett.* **371–372**, 177–190.

Jamieson R. A., Unsworth M. J., Harris N. B., Rosenberg C. L. and Schulmann K. (2011) Crustal melting and the flow of mountains. *Elements* **7**, 253–260.

Jordan T. H. (1988) Structure and formation of the continental tectosphere. *J. Petrol.* **Special_Volume**, 11–37.

Karlstrom L., Dufek J. and Manga M. (2010) Magma chamber stability in arc and continental crust. *J. Volcanol. Geoth. Res.* **190**, 249–270.

Kay R. W. and Mahlburg-Kay S. (1991) Creation and destruction of lower continental crust. *Geol. Rundsch.* **80**, 259–278.

Kelemen P. B. (1995) Genesis of high Mg# andesites and the continental crust. *Contrib. Miner. Petrol.* **120**, 1–19.

Korenaga J. (2013) Archean geodynamics and the thermal evolution of earth, archean geodynamics and environments. *Am. Geophys. Union*, 7–32.

Kruse S., McNutt M., Phipps-Morgan J., Royden L. and Wernicke B. (1991) Lithospheric extension near Lake Mead, Nevada: a model for ductile flow in the lower crust. *J. Geophys. Res. Solid Earth* **96**, 4435–4456.

Lee C.-T. A. and Bachmann O. (2014) How important is the role of crystal fractionation in making intermediate magmas? Insights from Zr and P systematics. *Earth Planet. Sci. Lett.* **393**, 266–274.

Lee C.-T. A. and Chin E. J. (2014) Calculating melting temperatures and pressures of peridotite protoliths: implications for the origin of cratonic mantle. *Earth Planet. Sci. Lett.* **403**, 273–286.

Lee C.-T. A. and Lackey J. S. (2015) Global continental arc flare-ups and their relation to long-term greenhouse conditions. *Elements* **11**, 125–130.

Lee C.-T. A., Morton D. M., Kistler R. W. and Baird A. K. (2007) Petrology and tectonics of Phanerozoic continent formation: from island arcs to accretion and continental arc magmatism. *Earth Planet. Sci. Lett.* **263**, 370–387.

Lee C.-T. A., Shen B., Slotnick B. S., Liao K., Dickens G. R., Yokoyama Y., Lenardic A., Dasgupta R., Jellinek M. and Lackey J. S. (2013) Continental arc–island arc fluctuations, growth of crustal carbonates, and long-term climate change. *Geosphere* **9**, 21–36.

Lee C.-T. A., Thurner S., Paterson S. and Cao W. (2015) The rise and fall of continental arcs: Interplays between magmatism, uplift, weathering, and climate. *Earth Planet. Sci. Lett.* **425**, 105–119.

Lee C. T. A. (2014) 4.12 – physics and chemistry of deep continental crust recycling. In *Treatise on Geochemistry (Second Edition)* (eds. H. D. Holland and K. K. Turekian). Elsevier, Oxford, pp. 423–456.

Lee C. T. A., Cheng X. and Horodyskyj U. (2006) The development and refinement of continental arcs by primary basaltic

Please cite this article in press as: Tang M., et al. Rapid mantle convection drove massive crustal thickening in the late Archean. *Geochim. Cosmochim. Acta* (2019), https://doi.org/10.1016/j.gca.2019.03.039

magmatism, garnet pyroxenite accumulation, basaltic recharge and delamination: insights from the Sierra Nevada, California. *Contrib. Miner. Petrol.* **151**, 222–242.

Martin H. (1986) Effect of steeper Archean geothermal gradient on geochemistry of subduction-zone magmas. *Geology* **14**, 753–756.

Martin H. and Moyen J.-F. (2002) Secular changes in tonalite-trondhjemite-granodiorite composition as markers of the progressive cooling of Earth. *Geology* **30**, 319–322.

Martin H., Smithies R., Rapp R., Moyen J.-F. and Champion D. (2005) An overview of adakite, tonalite–trondhjemite–granodiorite (TTG), and sanukitoid: relationships and some implications for crustal evolution. *Lithos* **79**, 1–24.

McKenzie N. R., Horton B. K., Loomis S. E., Stockli D. F., Planavsky N. J. and Lee C.-T. A. (2016) Continental arc volcanism as the principal driver of icehouse-greenhouse variability. *Science* **352**, 444–447.

Moyen J.-F. and Martin H. (2012) Forty years of TTG research. *Lithos* **148**, 312–336.

Moyen J.-F. and Stevens G. (2013) Experimental constraints on TTG petrogenesis: implications for archean geodynamics, archean geodynamics and environments. *Am. Geophys. Union*, 149–175.

O'Neill C., Lenardic A., Moresi L., Torsvik T. and Lee C.-T. (2007) Episodic Precambrian subduction. *Earth Planet. Sci. Lett.* **262**, 552–562.

Parman S. W. (2015) Time-Lapse zirconography: imaging punctuated continental evolution. *Geochem. Perspect. Lett.* **1**, 43–52.

Pearson D. G., Parman S. W. and Nowell G. M. (2007) A link between large mantle melting events and continent growth seen in osmium isotopes. *Nature* **449**, 202–205.

Pertermann M. and Hirschmann M. M. (2003) Partial melting experiments on a MORB-like pyroxenite between 2 and 3 GPa: Constraints on the presence of pyroxenite in basalt source regions from solidus location and melting rate. *J. Geophys. Res.: Solid Earth* **108**.

Pertermann M., Hirschmann M. M., Hametner K., Günther D. and Schmidt M. W. (2004) Experimental determination of trace element partitioning between garnet and silica-rich liquid during anhydrous partial melting of MORB-like eclogite. *Geochem. Geophys. Geosyst.* **5**, Q05A01.

Planavsky N. (2018) From orogenies to oxygen. *Nat. Geosci.* **11**, 9–10.

Presnall D. C. (1999) Effect of pressure on the fractional crystallization of basaltic magma. *Mantle Petrol.: Field Observ. High Press. Experiment.: Tribute Francis R. (Joe) Boyd Geochem. Soc. Special Publ.* **6**, 209–224.

Ringuette L., Martignole J. and Windley B. F. (1999) Magmatic crystallization, isobaric cooling, and decompression of the garnet-bearing assemblages of the Jijal sequence (Kohistan terrane, western Himalayas). *Geology* **27**, 139–142.

Roering J. J., Perron J. T. and Kirchner J. W. (2007) Functional relationships between denudation and hillslope form and relief. *Earth Planet. Sci. Lett.* **264**, 245–258.

Rudnick R. and Taylor S. (1986) Geochemical constraints on the origin of Archaean tonalitic-trondhjemitic rocks and implications for lower crustal composition. *Geol. Soc. London Special Publ.* **24**, 179–191.

Rudnick R. L. (1995) Making continental crust. *Nature* **378**, 571–578.

Rudnick R. L. and Fountain D. M. (1995) Nature and composition of the continental crust: a lower crustal perspective. *Rev. Geophys.* **33**, 267–309.

Rudnick R. L., McDonough W. F. and O'Connell R. J. (1998) Thermal structure, thickness and composition of continental lithosphere. *Chem. Geol.* **145**, 395–411.

Stein M. and Hofmann A. W. (1994) Mantle plumes and episodic crustal growth. *Nature* **372**, 63.

Sun S.-S. and McDonough W. F. (1989) Chemical and isotopic systematics of oceanic basalts: implications for mantle composition and processes. *Geol. Soc. London, Special Publ.* **42**, 313–345.

Tackley P. J., Stevenson D. J., Glatzmaier G. A. and Schubert G. (1993) Effects of an endothermic phase transition at 670 km depth in a spherical model of convection in the Earth's mantle. *Nature* **361**, 699.

Tang M., Chen K. and Rudnick R. L. (2016) Archean upper crust transition from mafic to felsic marks the onset of plate tectonics. *Science* **351**, 372–375.

Tang M., Erdman M., Eldridge G. and Lee C.-T. A. (2018) The redox "filter" beneath magmatic orogens and the formation of continental crust. *Sci. Adv.* **4**.

Tang M., Lee C.-T. A., Chen K., Erdman M., Costin G. and Jiang H. (2019) Nb/Ta systematics in arc magma differentiation and the role of arclogites in continent formation. *Nat. Commun.* **10**, 235.

Tang M., Rudnick R. L., McDonough W. F., Gaschnig R. M. and Huang Y. (2015) Europium anomalies constrain the mass of recycled lower continental crust. *Geology* **43**, 703–706.

Turcotte D. L. and Schubert G. (1982) *Geodynamics: Applications of Continuum Physics to Geological Problems*. John Wiley, New York, 450p.

Voice P. J., Kowalewski M. and Eriksson K. A. (2011) Quantifying the timing and rate of crustal evolution: global compilation of radiometrically dated detrital zircon grains. *J. Geol.* **119**, 109–126.

Wang H., van Hunen J. and Pearson D. G. (2016) Making Archean cratonic roots by lateral compression: a two-stage thickening and stabilization model. *Tectonophysics*.

Wang Y., Zhang J., Jin Z. and Green H. (2012) Mafic granulite rheology: implications for a weak continental lower crust. *Earth Planet. Sci. Lett.* **353**, 99–107.

Zimmer M. M., Plank T., Hauri E. H., Yogodzinski G. M., Stelling P., Larsen J., Singer B., Jicha B., Mandeville C. and Nye C. J. (2010) The role of water in generating the calc-alkaline trend: new volatile data for Aleutian magmas and a new tholeiitic index. *J. Petrol.* **51**, 2411–2444.

Associate Editor: Fang-Zhen Teng

Please cite this article in press as: Tang M., et al. Rapid mantle convection drove massive crustal thickening in the late Archean. *Geochim. Cosmochim. Acta* (2019), https://doi.org/10.1016/j.gca.2019.03.039